Article

Structural Decoding of a Small Molecular Inhibitor on the Binding of SARS-CoV-2 to the ACE 2 Receptor

Pushpendra Mani Mishra and Chayan Kanti Nandi*

Read Online

ACCESS | 📊 Metrics & More | 📰 Article Recommendations | 🆂�🅸 Supporting Information

ABSTRACT: Inhibition of the interaction of the receptor-binding domain (RBD) of the spike protein and the human angiotensin-converting enzyme 2 (ACE 2) receptor is the most effective therapeutic formulation to restrict the contagious respiratory illness and multiple organ failure caused by the novel SARS-CoV-2 virus. Based on the structural decoding of the RBD of the spike protein, here we have generated a new set of small molecules that have strong inhibiting properties on the binding of the spike protein to ACE 2 receptors. These small-molecule inhibitors surprisingly show binding to the main protease, nucleoprotein, and RNA-dependent RNA polymerase, which are the other responsible factors for the viral infection. The newly designed molecules show better performance than several existing repurposed drugs. Conformational changes from closed to closed lock and open conformations of the SARS-CoV-2 binding to the ACE 2 receptor were observed in the presence of these small molecular inhibitors, suggesting their strong abilities to counteract the SARS-CoV-2 infection.
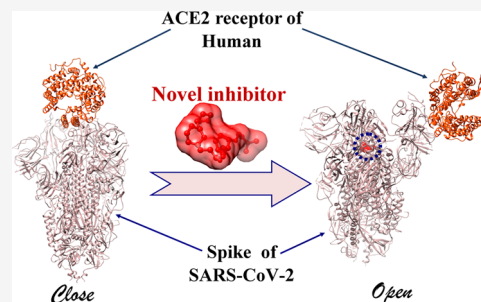
INTRODUCTION

Severe acute respiratory syndrome coronavirus 2 (SARS-CoV-2) has infected more than 100 million people along with a total death of over 2.5 million people worldwide.[1] Considering the severity of SARS-CoV-2 infection, an urgent need for a vaccine and chemotherapeutic drug development is of utmost importance.[2] Toward this goal, an impressive outcome of more than 60 vaccines has been achieved against SARS-CoV-2 infection.[3] Although few of them showed promising results against the viral infection, several adverse outcomes among vaccine recipients have led to the release of a factsheet by the manufacturers. Recent investigation indicated that the antibody therapy in patients could be detrimental to their health in addition to harboring the potential for mutating the virus.[4] On the other hand, drug repurposing with the existing available drugs has also been exploited to treat the worsening condition of patients infected with SARS-CoV-2[5] or hold high promise in doing so.[6,7] To name a few, remdesivir, hydroxychloroquine, chloroquine, ribavirin, and lopinavir are the most commonly used drugs available in the market.[8] However, with their few promising outcomes on viral treatment, severe side effects such as cardiotoxicity, gastrointestinal effects, hypokalemia, self-limited skin eruption, retinopathy, and fatality in critically ill patients have restricted their use in general.[9−12]

A full-length SARS-CoV-2 virus that is encoded by the ∼30 Kb positive-sense single-stranded RNA consists of several structural, non-structural, and accessory proteins, which are responsible for their distinct functions on the viral infection (Figure 1a). The four main structural proteins are spike (S), membrane (M), envelop (E), and nucleocapsid (N) proteins along with 16 non-structural proteins (nsp 1−16) and accessory proteins (ORF 3a, 3b, 6, 7a, 7b, 8b, 9b, and 14).[13,14] The S protein ectodomain of all CoV is classified into two subunits S1 and S2. The S1 subunit consists of the N-terminal domain and C-terminal domain. Both the domains can function as a receptor-binding domain (RBD) and are also competent in binding to numerous proteins and sugars. The S2 subunit's functional role is the fusion of the virus to host cells. It consists of putative fusion peptides and heptad repeats.[15] Domains and important regions of S protein are depicted in a linear bar representation and marked on the single chain of S protein in Figure 1a,b, respectively. Three single S proteins assemble to form a trimeric spike protein (Figure 1c). Spike glycoprotein (S) is responsible for the interaction of the virus to the host cells via its RBD and further facilitates its fusion and entry into the host cells. The binding of the RBD of the S protein to the ACE 2 cell receptor is supposed to be the most crucial factor for viral entry, replication, maturation, and infection.[16] Restricting the virus from binding to ACE 2 receptors, blocking the host's specific receptors or enzymes, and preventing viral replication and RNA synthesis are among several other ways to inhibit the viral infection.[17]
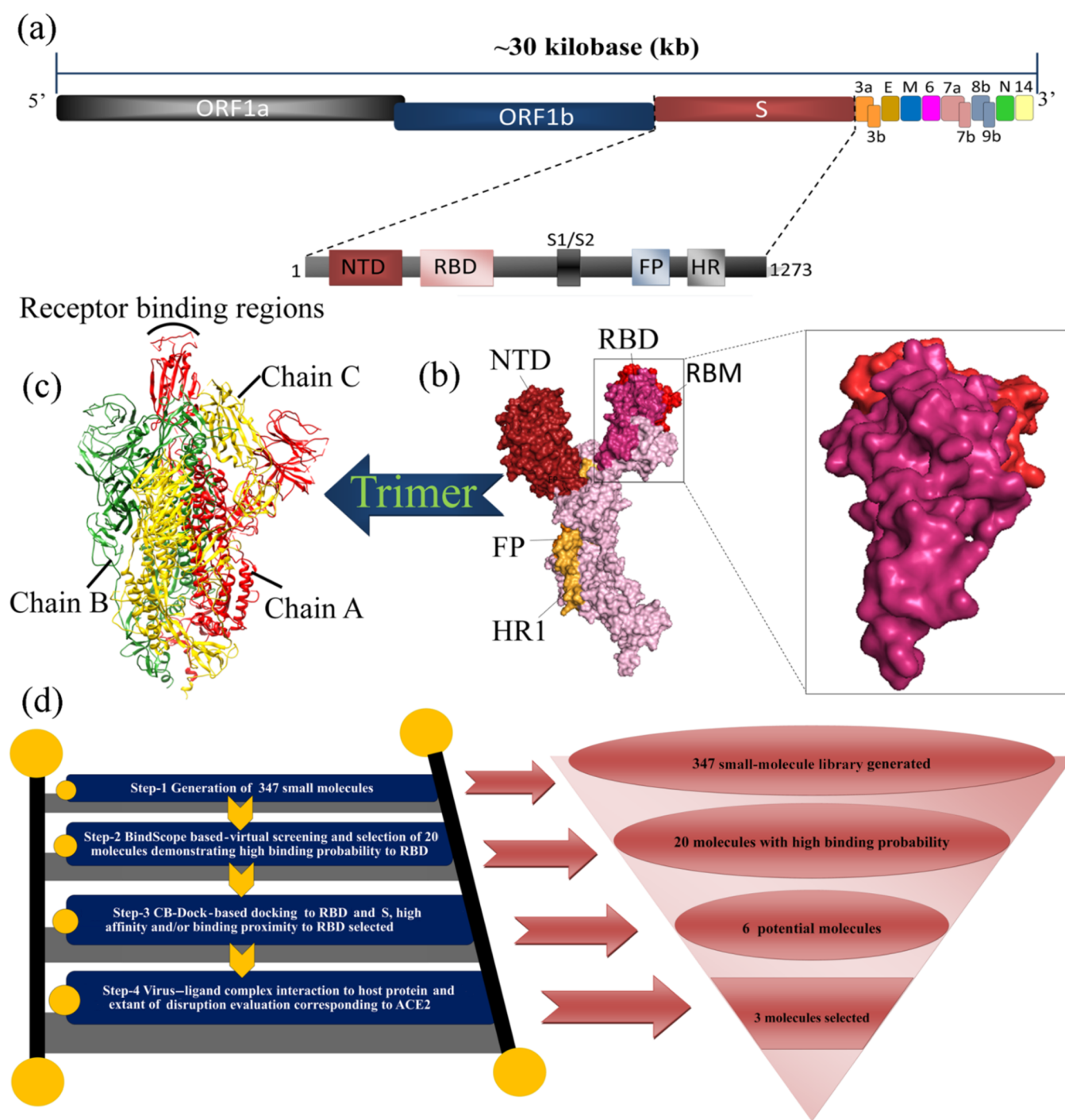
Despite many experimental and computational studies currently ongoing, to date, there is no confirmed effective
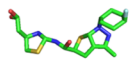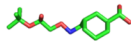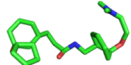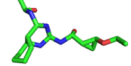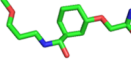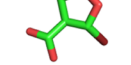
Figure 1. (a). Schematic representation of the SARS-CoV-2 genomic organization and its spike protein functional domains (RBD: receptor binding domain and NTD: N-terminal domain); important regions are the S1 and S2 subunits, FP: fusion peptide, and HR: heptad repeat. (b) Surface view of a single chain of the spike protein with marked positions of domains (RBD and NTD), the external subdomain containing RBM, the receptor binding motif, and important regions (FP and HR). (c) Cartoon view of the trimeric spike protein whose individual chain is colored in different colors. (d) Process and techniques utilized to identify the potential novel small-molecule inhibitors.

treatment available against SARS-CoV-2 infection.[18] As a result, there is a dire need to design and develop new drug molecules with better performance to get rid of the infection. The 3D structure of RBD consists of a core and extended insertion regions. The core is formed by five stranded antiparallel beta sheets ($\beta1-\beta4$ and $\beta7$), while the extended insertion region, also called RBM, is formed between $\beta4$ and $\beta7$ by $\beta5$ and $\beta6$ strands, two helices, and a loop. RBM consists of the most interacting residues while binding to ACE 2. RBM's extended concave outer surface interacts with the bottom side of the small lobe of ACE 2, accommodating its N-terminal helices. The holding up of the ACE 2 helices by the RBM outer surface results in a large buried surface area of 1687 Å^2 at the RBD−ACE 2 interface, of which 864 Å^2 area is on the RBD side while 823 Å^2 is on the ACE 2 side.[19] Upon interaction with ACE 2, the spike protein trimer undergoes a conformational change, allowing the S1 and S2 cleavage site to host protease. Cleavage of S1 and S2 results in priming of the membrane fusion of the spike protein by enabling

Scheme 1. Newly Identified Small-Molecule Inhibitors (NISM 1−NISM 6), Their Structure, IUPAC Name, Chemical Formula, and Molecular Weight

Ligands	Molecular structure	IUPAC Name	Chemical formula	Molecular weight
NISM1		2-(2-(1-(4-fluorophenyl)-3-methyl-1H-thieno[2,3-c]pyrazole-5-carboxamido)thiazol-4-yl)acetic acid	$C_{18}H_{13}FN_4O_3S_2$	416.45
NISM2		3-(((2-(tert-butoxy)-2-oxoethoxy)imino)methyl)benzoic acid	$C_{14}H_{17}NO_5$	279.29
NISM3		3-(3-(cyclopentyloxy)phenyl)-N-(2-(2-(dimethylamino)ethoxy)benzyl)propanamide	$C_{25}H_{34}N_2O_3$	410.56
NISM4		N-(4-acetamidoquinazolin-2-yl)-2-ethoxycyclopropane-1-carboxamide	$C_{16}H_{18}N_4O_3$	314.35
NISM5		3-(2-amino-2-oxoethoxy)-N-(3-methoxypropyl)benzamide	$C_{13}H_{18}N_2O_4$	266.30
NISM6		2-bromofuran-3-carboxylic acid	$C_5H_3BrO_3$	190.98

the insertion of the FP domain of S2 into the membrane. This causes the formation of a six-heptad bundle (6-HB) between two heptad repeats. 6-HB stabilizes the conformational change in the S2 subunit, which is in close proximity to the viral and host membranes and effectively triggers the membrane fusion of the spike.[20] As a result, the structural decoding of the RBD to circumvent the interaction between the spike protein and the ACE 2 receptor will be a crucial factor.

In the current work, to identify the potential novel small molecules, the structure associated with the geometrical, chemical, and evolutionary properties of the RBD is decoded first for the generation and selection of small molecules. Based on the structural decoding, we generated a new set of small molecules, which showed good inhibiting properties against spike protein and ACE 2 host cell receptors. These molecules also strongly bind with the main protease (MPro), nucleoprotein, and RNA-dependent RNA polymerase (RDRP) and thus show diverse applications in restricting viral infection. We have compared the binding affinities of these small molecules with several FDA-approved drugs. The screened small molecules were proven to be either equally or more effective than the FDA-approved drugs. Interestingly, upon interaction with these selected small molecular drugs, the spike protein ACE 2 complex was found to change conformation. In the native form, ACE 2 interacts with the RBD in a closed conformation with a high binding affinity, whereas the ligand-bound spike protein seems to interact with ACE 2 in a closed lock conformation or an open conformation. The ligand-altered conformation is either open or closed lock, and both forms have the potential for effective inhibition of the viral infection.[21] Several computation tools and techniques as shown in Figure 1d (details of the codes used for the study are provided in the Supporting Information) were exploited to show the effectiveness of these molecules.

MATERIALS AND METHODS

**Shape-Decoded Molecule Generation and Virtual Screening.** Cavity coordinates in the RBD (in PDB ID: 6M17) of the virus were detected using DeepSite[22] and further submitted to the LIGANN server[23] for the generation of the shape-decoded molecular library. High-throughput screening of these novel molecules in binding to the virus RBD was performed using BindScope,[24] and molecules demonstrating high binding probability were selected for further examination.

Novel Molecule Docking, Simulation, Drug-Likeness, and Virus−Host Interaction Influence. The CB-Dock[25] server was used to perform the detailed docking of selected molecules to the full spike protein, several viral components, and ACE 2 receptor. Drug-likeness of these novel molecules was identified using Swiss-ADME,[26] and molecules demonstrating a high docking score or binding proximity to the RBD (when docked with the spike) were selected for molecular dynamics (MD) simulation and virus−host protein interaction impact analysis. LARMD[27] server-directed MD simulation and PatchDock[28] and FireDock[29] server-based disruption analyses of virus−protein interaction (SARS-CoV-2 spike−ACE 2 receptor of humans) were performed.

Pharmacological Property Exploration. The pharmacological property and safety parameters of selected ligands and existing antivirals currently employed in SARS-CoV-2 treatment were assessed using the Osiris property explorer tool.[30]

RESULTS AND DISCUSSION

Structural Decoding and Ligand Generation. At first, based on a few parameters such as the excluded volume, hydrogen bond acceptor/donor, aromaticity, hydrophobicity, metallic character, and ionization energy, we have generated favorable and accessible binding pockets in the RBD of the spike protein (protein data bank ID 6M17) using the deep convolution neural network (DCNN) model.[22] The necessary preparation of the protein structure data for an effective computational outcome was performed using Pymol software. Using the DeepSite server,[22] four different types of binding pockets of varying strengths in the RBD were obtained (Figure S1a). The DeepSite machine learning algorithm is based on a DCNN that is superior to other competitive methods without encoding any problem-specific knowledge.[22] A computationally
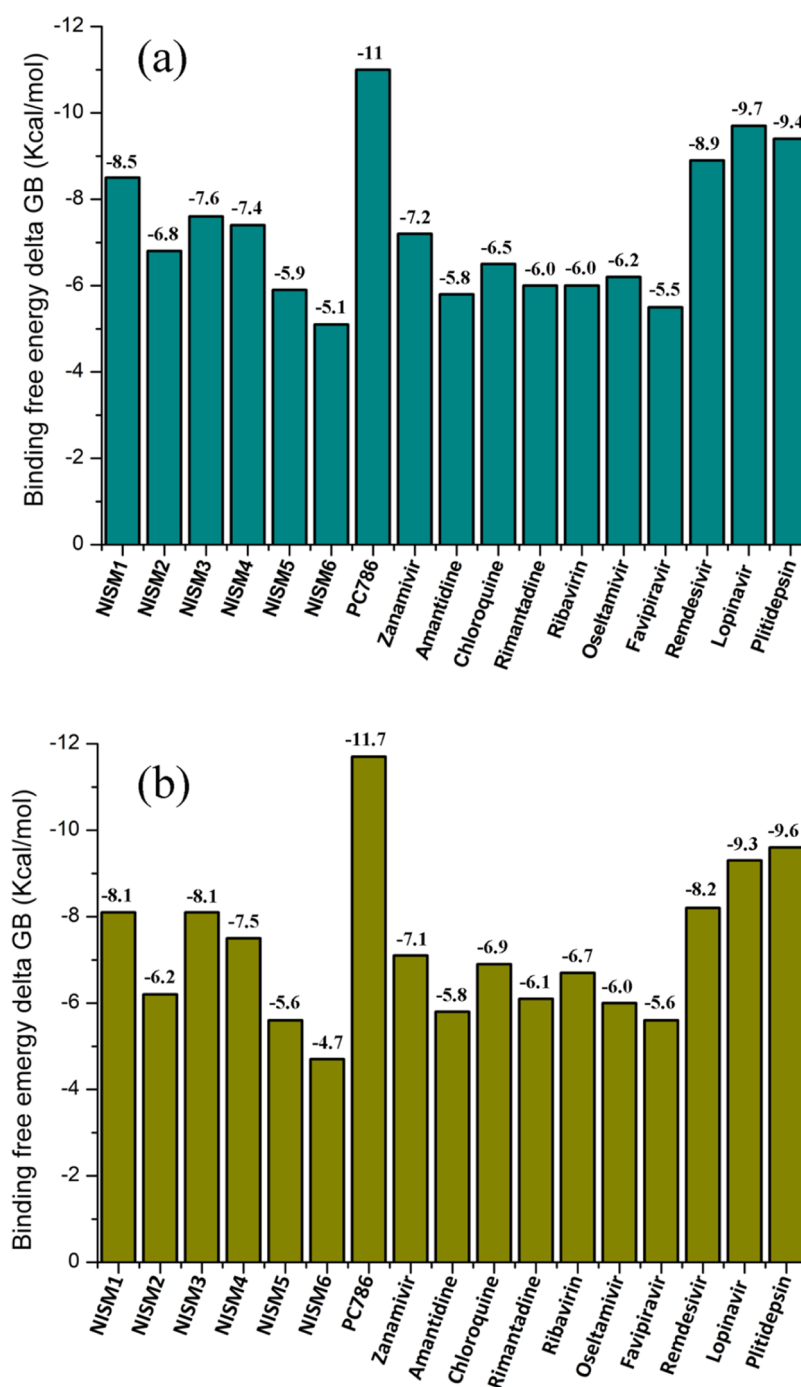
Figure 2. Comparison of binding free energy change of NISMs with known drugs using CB-Dock. (a) Bar graph of energy values for binding of ligands to the spike protein of SARS-CoV-2 shown in olive color. (b) Bar graph of energy values for binding of ligands to the host receptor ACE2 in khaki color.

predicted score is assigned to each of the pockets for measuring their binding strength toward small molecules. The scores being close to unity suggest the goodness of the binding pockets.[22] A grid box around each of the binding pockets was created (Figure S1b) in the generative neural network-based LIGANN server[23] to generate structural decoded de novo drug molecules. The shape-captioning network decodes the shape of the ligands into simplified molecular input line entry system (SMILES) strings.[23,31,32] Based on the structural information of all four cavities, a total of 347 ligands in the SMILES string were generated. Once the SMILE string of small molecules is generated, the file containing the string is submitted to

BindScope[24] for virtual screening. Similar to DeepSite, the BindScope server is also based on a DCNN and performs large-scale classification of submitted ligands into active and inactive compounds. The binding probabilities obtained from the server are summarized in Tables S1−S4. After screening all 347 ligands via the high-throughput screening server, we obtained the top 20 molecules with a high probability of binding (Table S5).

Molecular Docking and Screening of Ligands. The aforementioned 20 molecules were subjected to further detailed screening using the CB-Dock server.[25] This is a user-friendly blind docking server that predicts the binding of a submitted protein and provides docking output with a popular docking
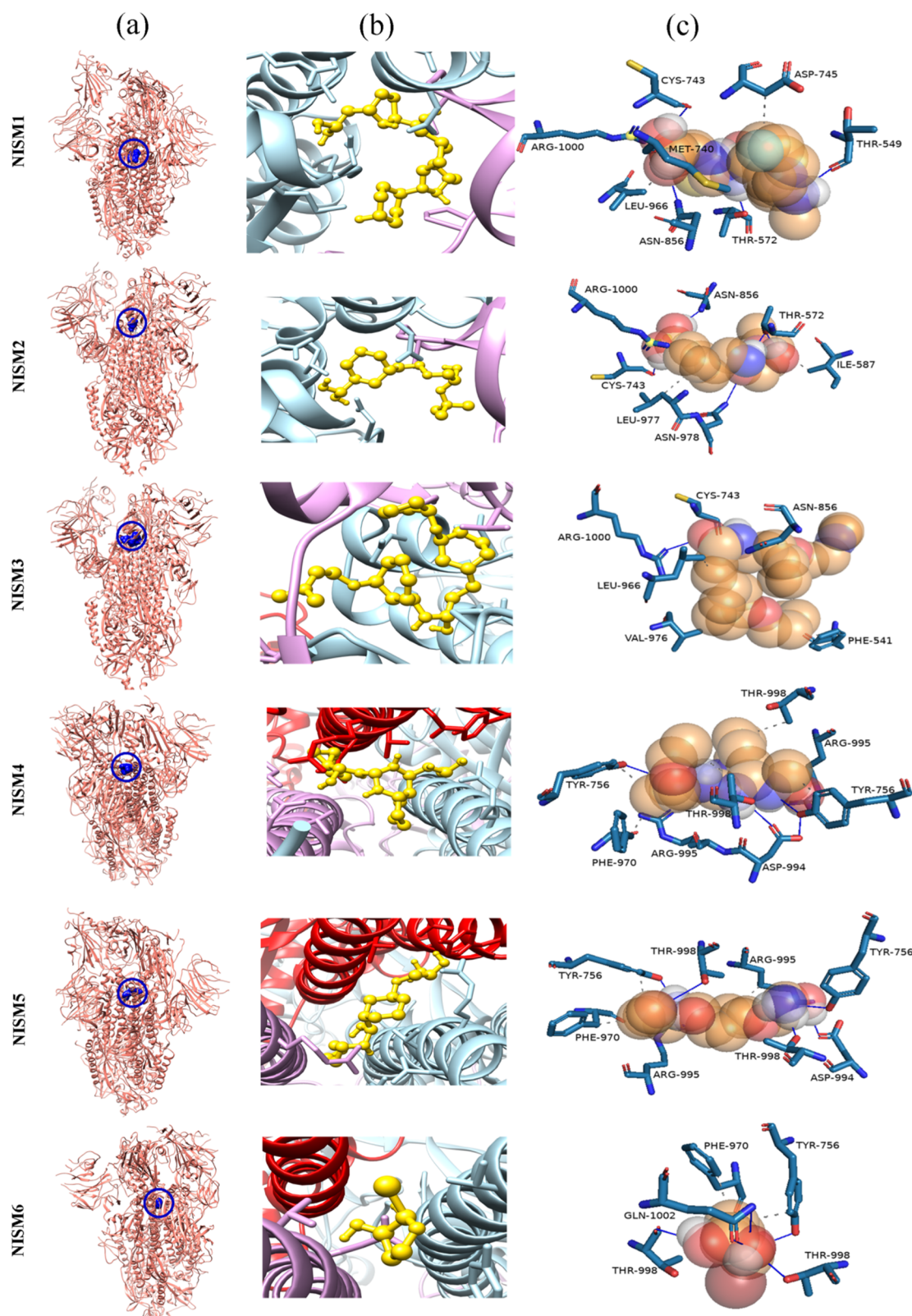
Figure 3. Visualization of ligands (NISM1−NISM 6) binding to trimeric S of SARS-CoV-2 and their conformation and protein residue interaction details. (a) Ligand-binding site in the trimeric spike protein of SARS-CoV-2; the bounded site is encircled in blue color. (b) Bounded conformation of ligands in yellow color to the viral spike protein whose different chains (A−C) are colored in red, violet, and light blue colors respectively. (c) Amino acid residues of protein in blue color interacting with ligand molecules (shown in a spherical representation and colored in red, white, and blue).

program, AutoDock Vina.[33] The screening resulted in a broad range of binding affinity toward both the RBD and full spike proteins. Finally, the six best molecules (NISM1, NISM2, NISM3, NISM4, NISM5, and NISM6) (Scheme 1), which showed the best potential to inhibit the spike protein−ACE 2 interaction, were chosen for further study.
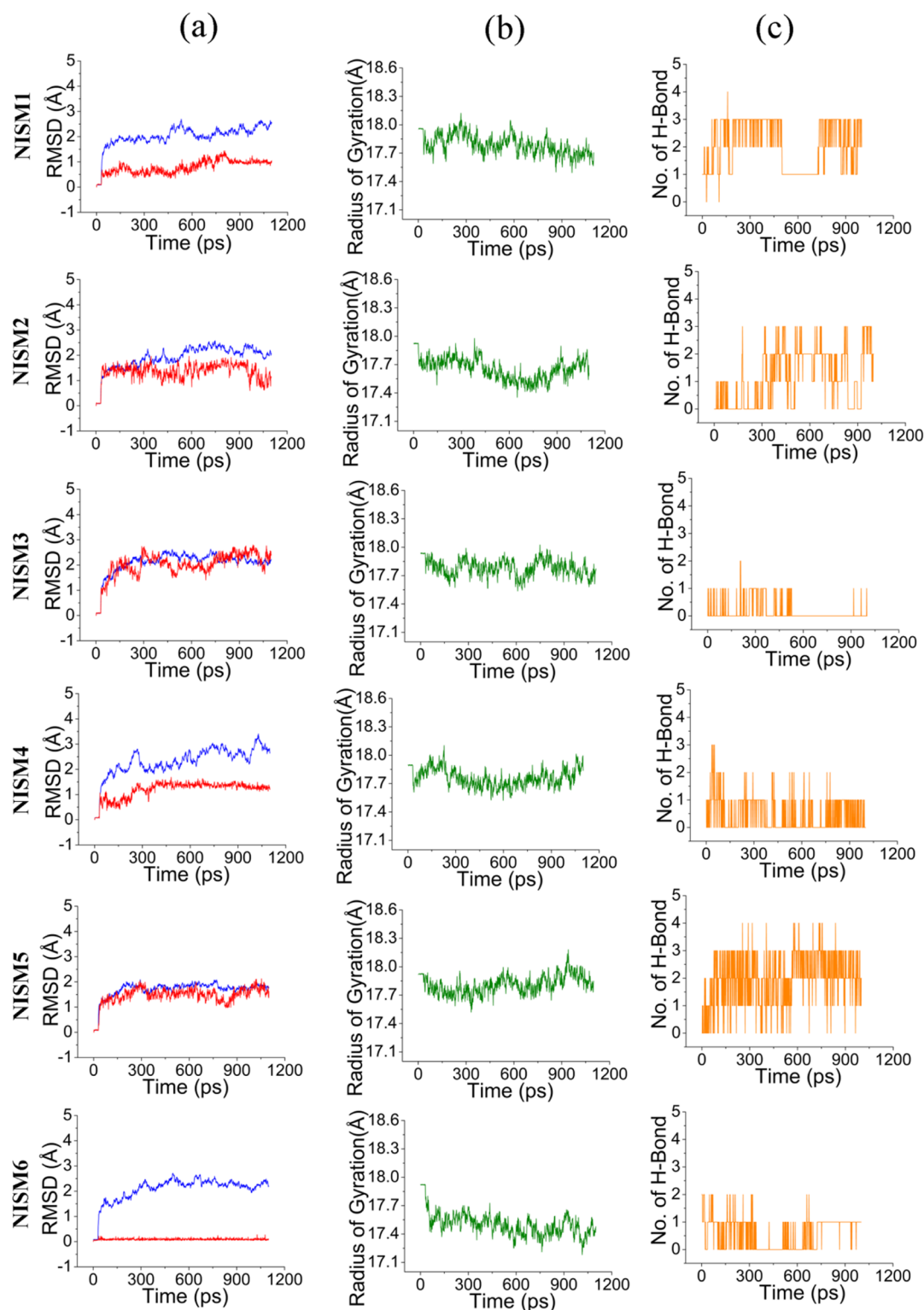
Figure 4. MD simulation of NISMs with the RBD of spike protein in a 1 ns simulation study. (a) RMSD of the receptor (blue color) and ligand (red) well within or around 2 Å. (b) Compactness change of the ligand protein complex is analyzed by R_g as shown in column b, a low change in R_g demonstrating high stability of complexes. (c) Formation and disruption of a hydrogen bond with respect to a small time fraction.

The molecular docking analysis revealed that these newly developed small molecules have binding energies within the range from −5.1 to −8.5 kcal/mol with S protein (Table S6). It is to be noted here that the binding energies obtained for these molecules, especially NISM1, NISM3, and NISM4, with the spike protein (PDB ID: 6VSB) and host receptor ACE 2 (PDB

ID: 1r42) are highly similar or provide better binding than that of several other approved drugs (Figure 2a,b). In addition, we also carried out the docking of these ligands with the MPro (PDB ID: 6LU7), nucleoprotein RNA-interacting region (PDB ID: 6VYO), nucleoprotein dimerization region (PDB: ID 6YUN), and RDRP complex (PDB: ID 6M71). In all these
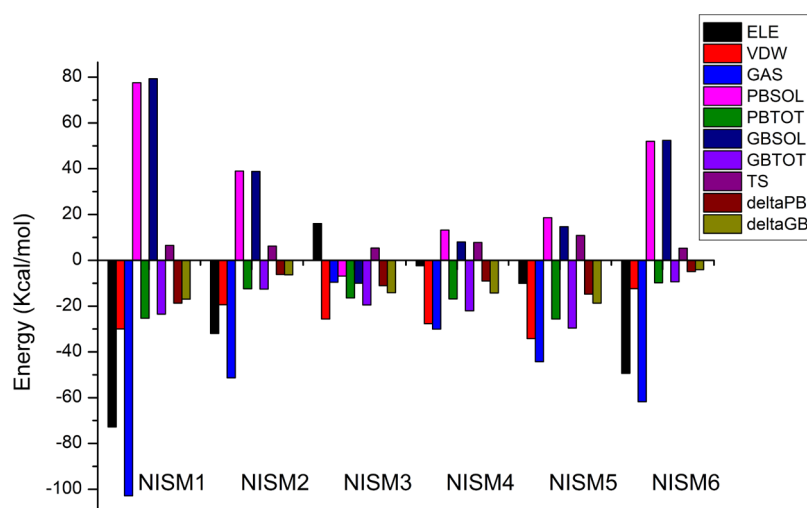
Figure 5. MM,/PB(GB)SA calculated energy plot of selected ligands (NISM1−NISM 6) bounded to the RBD; the energy plot consists of electrostatic energy (ELE), Van der Waals (VDW) contribution, total gas phase energy (GAS), non-polar and polar contributions to solvation (PBSOL/GBSOL), entropy (TS), PB total (PBTOT), GB total (GBTOT), change in binding energy by the P method (delta PB), and change in binding energy by the G method (delta GB), shown in different colors.

target biomolecules, the binding energy was found to be in the range from −4.4 to −8.5 kcal/mol (Table S6).

The CB-Dock output data analysis results of selected ligands are shown in Figure 3. In the given figure's first column, we have shown the small-molecule binding locations in the trimeric S protein, encircled by blue color. The second column shows the close view of the binding site and docked conformation of small molecules, and finally, the third column shows the amino acid residues that bind with the small molecules. NISM1 was used to bind due to its hydrophobic, hydrogen bonds and salt bridge interaction (hydrophobic: ASP745 and LEU966; hydrogen bonding: THR549, THR572, MET740, CYS743, and ASN856, and salt bridge: ARG1000) and provided the maximum stable binding (Table S7). NISM 2, although showing strong hydrophobic and hydrogen bond interaction (hydrophobic: ILE587 and LEU977; hydrogen bonding: THR572, CYS743, ASN856, and ASN978) with the same binding pocket as that used for NIMS1, showed a little lower binding energy as it does not contain salt bridge interaction. On the other hand, NISM4 and NISM5 showed high numbers of hydrophobic and hydrogen bond interactions with a few similar types of amino acid residues (Table S7) in the same binding pocket, which is different from the binding pocket of NISM1 and NISM2. From the above results, it could be suggested that along with hydrogen bonding and hydrophobic interaction, the salt bridge interaction played a key role in NISM1 for its enhanced binding energy. NISM 5 and NISM6 showed comparatively low binding energy than all other NISMs, but they showed promising results as an efficient drug molecule, as discussed later.

MD Simulation. Next, we carried out the MD simulation to understand the protein−ligand interaction dynamics at an atomic level and in a small time fraction. The Amber16 software-based LARMD server was used with a standard protocol for the preparation of the structure, development of force field libraries, tunnel detection, and running of biased and unbiased MD simulations for investigating the ligand−protein interaction binding mode and dynamical unwinding processes.[27] LARMD was developed for a specific aim of solving the problem of profiling ligand-driven protein dynamics, and for such operations, it integrates several standard software packages

such as AMBER 16, MDTraj, R, ChemAxon, J.Smol, MolScript, and CAVER3.0.[27] Protein−ligand interaction analysis was performed using the interactional binding mode. The parameters such as root-mean-square deviation (rmsd), the radius of gyration (R_g), and the change in hydrogen bonding were checked for the validation of the ligand−protein interaction. The RBD of the spike proteins was used for the MD simulation. Figure 4 demonstrates the MD simulation output of all the six selected small molecules. The molecules bound to the RBD seem to fluctuate in the rmsd range within 2 Å for all the ligands, as displayed in the first column. The rmsd value within this limit suggests a good equilibrium structure without undergoing any conformation deviation of the RBD in the presence of the molecules. This was further confirmed by the R_g value (second column) for each of these molecules. The R_g value suggests no compaction or decompaction of the protein structure from its centroid within the time scale. The change in hydrogen bonding statistics and hydrogen bond formation was also observed in all cases. The number of hydrogen bond formation varied from zero to four in all cases. Such a large number of hydrogen bond formations almost in all the NISMs suggest their binding with the RBD of spike proteins with high stability.

For a better understanding of the binding energetics and to calculate the interaction-free energies of the ligand and RBD complex, molecular mechanics/Poisson Boltzmann (general-ized Born) surface area [MM-PB(GB)SA] calculations were carried out. The binding energy contributions such as polar and non-polar contributions to solvation (PBSOL/GBSOL), van der Waals (VDW) contribution, gas-phase energy (GAS), and entropy (TS) were calculated separately and later combined to get the total binding energies for each ligand. The detailed energetics has been presented in Figure 5 (and Table S8). It could be seen that apart from NISM 2 and NISM 6, all the ligands possess a very high binding energy, varying from −11.635 to −17.825 kcal/mol in MD simulation, thus suggesting their stable binding to the RBD.

Ligand-Mediated Disruption of Virus−Host Interaction. Analysis of the protein−protein interaction between the trimeric S protein and the ACE 2 receptor and the change in
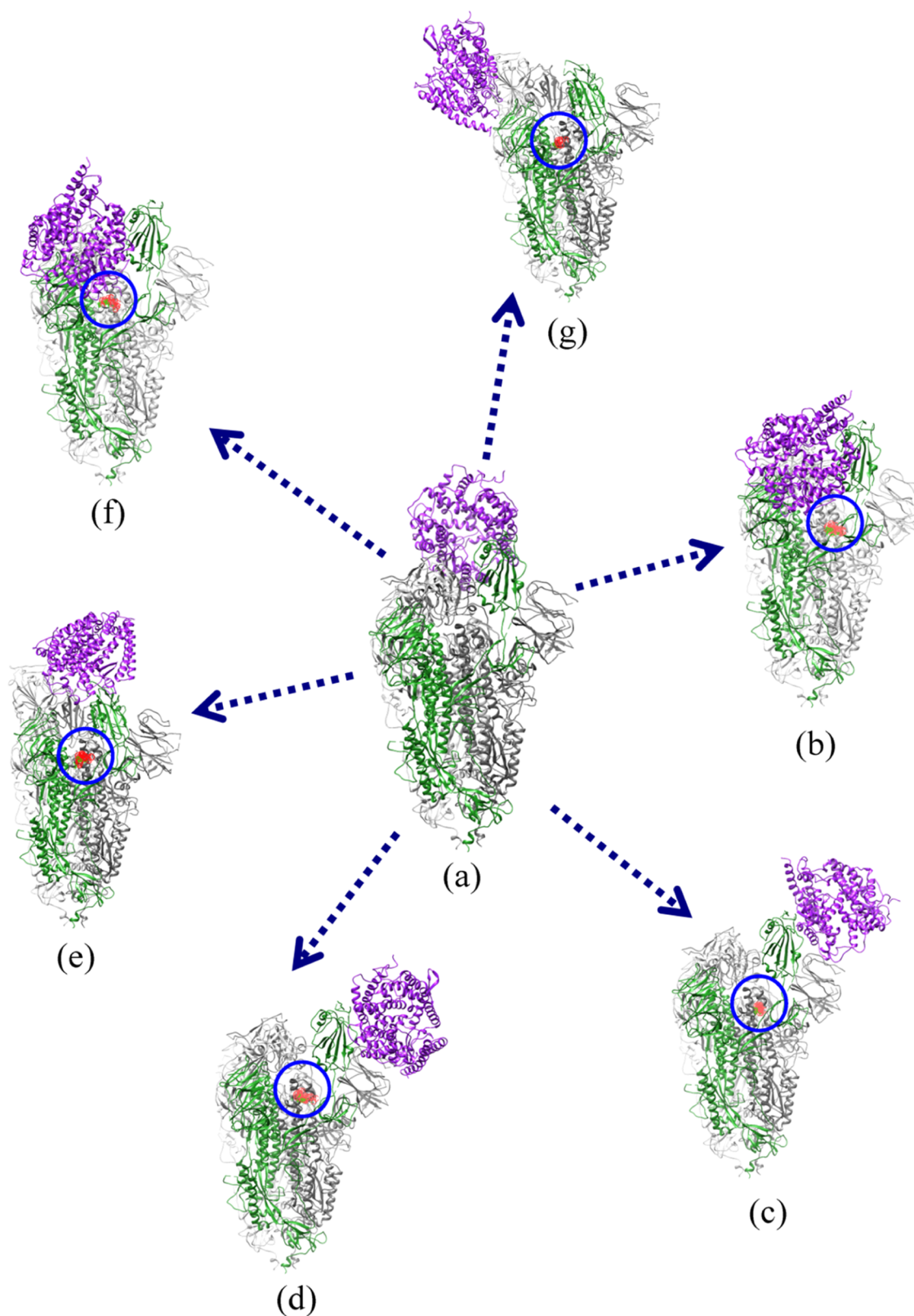
Figure 6. Diagrammatic representation of closed (native and disrupted locked binding site) and open (destabilize) conformations of interaction between SARS-CoV-2 trimeric S (chain A in green color, chain B in dark gray color, and chain C in light gray color) and the human ACE 2 receptor (violet color). (a) Close conformation interaction between virus trimeric S and the human ACE 2 receptor; (b–g) closed lock or open conformation interaction between trimeric S and the ACE 2 receptor where spike conformation altered by ligands NISM 1–NISM 6 (encircled in blue-color ring).

their conformations and binding affinity in the presence of all the NISMs was carried out to check the conformational change of the proteins. The PatchDock server[28] was used for the

calculation. Trimeric S proteins in their native form and while complexed with small molecules were used to compare their interactability differences with the ACE 2 receptor. PatchDock is
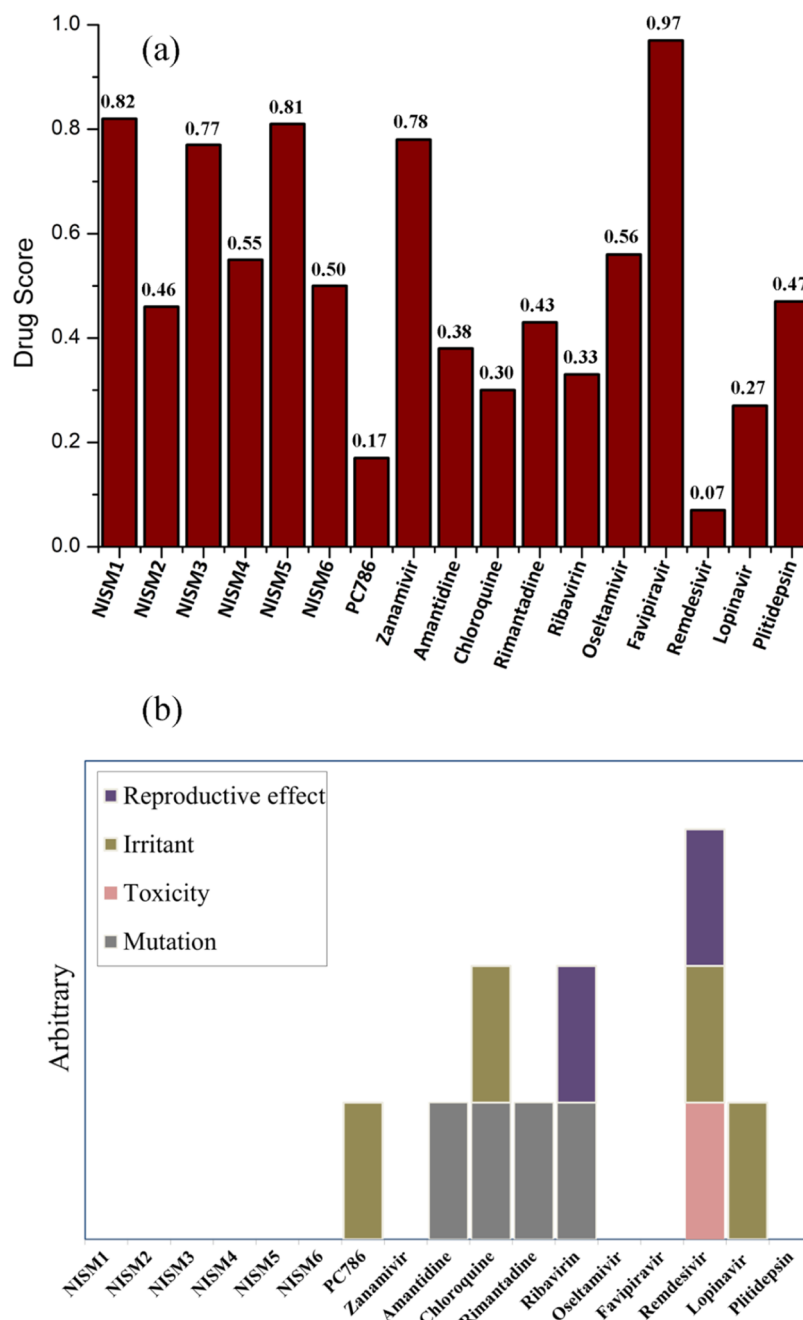
Figure 7. (a) Comparison of drug scores and (b) comparison of mutagenicity, toxicity, irritation, and reproductive effect of novel molecules and repurposed drugs. Comparative analysis reveals the high drug score and no mutagenicity, toxicity, irritation, and reproductive effect of novel ligands in comparison to that of most of the existing antiviral and repurposed drugs.

a geometry-based molecular docking algorithm to find the excellent molecular complementarity between interacting molecules. The set of rules was applied in filtering the redundant output including the geometric fit, atomic desolation, and rmsd. The high accuracy of PatchDock is driven by its fast molecular transformation searches backed by the local feature matching, advanced data structure, and spatial pattern recognition.[28] The FireDock server[34] was used to refine and obtain the best interaction model of the protein–protein interaction. The FireDock server is based on the algorithm that first performs the side-chain optimization, then performs rigid body minimization, and lastly provides the scoring and ranking based on the binding energy functions such as the desolvation energy, VDW

interaction, electrostatics, hydrogen and disulfide bonds, pi-stacking, aliphatic interaction, and rotamer's probabilities, and more.[29,34] Figure 6a shows the complex of the ACE 2 receptor (Violet color) with trimeric S (chain A green color, chain B in dark gray color, and chain C in light gray color) in a native or stable closed conformation. Figure 6b–g shows the destabilized or open conformation of a complex of ACE 2 to spike protein upon small-molecule interaction. The ligand binding in trimeric S pockets leads to conformation interference that ultimately causes the destabilization between SARS-Cov-2 and the ACE 2 receptor. Description of residue interaction between the protein spike and ACE 2 in both closed and open conformations is given in the Supporting Information and shown in Supporting

Information Figure S3. Small-molecule binding to a pocket of spike protein modulates the interaction force. As a result, structural modification leads to the disruption of trimeric spike protein binding to the ACE 2 receptor. The extent of alteration in the interaction between amino acids of the spike and ACE 2 was proportional to the structural and chemical properties of the small molecules bound to the spike protein. The stability of the complex of the spike and ACE 2 in both native and ligand-disrupted states is measured in terms of the atomic contact energy (ACE), which is a measure of the atomic desolvation energy defined over the energy of replacing protein−atom/water contact with protein−atom/protein−atom contact in the formation of a protein−protein complex. A lower ACE value describes a lower desolvation-free energy, which is more favorable.[35] The ACE value of spike−ACE 2 in the native state was 3.31, while for the ligand (NISM 1−NISM 6)-disrupted spike−ACE 2 complex, the ACE values were 13.54, −5.8, 1.6, 5.74, 13.77, and 1.6, respectively. The low ACE of the ligand-disrupted complex than the ACE of the native form indicates the high stability in the deformed state, while the higher ACE of the ligand-deformed complexes is indicative of their comparatively less stability than that of the native complex. Thus, the result suggested that a few molecules provide a more stabilized closed pack conformation, while a few of them showed open destabilized conformations. Similar closed and open conformational changes were recently observed for fatty acid binding on the spike protein.[19]

Pharmacological Property Analysis and Comparison. Finally, we have assessed the pharmacological properties of these six molecules and compared them with those of known antivirals and drugs currently repurposed for SARS-CoV-2 neutralization. Osiris property explorer[30] is an in-house-developed informatics system for drug discovery; the online web server allows the assessment of drug parameters such as LogP, solubility, molecular weight, drug score, mutagenicity, tumorigenic potential, irritant response, reproductive effect, and other parameters such as the number of hydrogen bond acceptors and donors. The drug score is calculated from eq 1 by multiplying the contribution of individual properties.

$$ds = \prod \left(\frac{1}{2} + \frac{1}{2}si \right) \cdot \prod ti \tag{1}$$

$$s = \frac{1}{1 + e^{ap+b}} \tag{2}$$

In eq 1, ds is the drug score and Si is the contribution calculated from Log P, Log S, M_{wt} and drug-likeness (Pi) via the given second equation that describes a spline curve. a and b in eq 2 have fixed values (1, −5), (1, 5), (0.012, −6), and (1, 0) for Log P, Log S, M_{wt}, and drug-likeness, respectively. In eq 1, ti is the contribution from four types of toxicity risk. The fixed values for high, medium, and no risk toxicity parameters are 0.6, 0.8, and 1, respectively. We have investigated the aforementioned properties and compared their results with those of known antiviral/drugs repurposed for COVID-19 treatment. Interestingly, NISM 1, NISM 3, and NISM 5 showed excellent drug scores (Figure 7 and Table S9). They are much superior to any other reported drug except favipiravir. Interestingly, the NISMs showed no toxicity, mutagenic effect, no irritant response, and no reproductive effect, while almost all the reported drugs have one or more negative effects except zanamivir, oseltamivir, and favipiravir.

CONCLUSIONS

In conclusion, in this work, we have generated a new set of small molecules that have strong inhibition potential against the binding of the spike protein and ACE 2 receptor. These small molecules also showed strong binding to the MPro, nucleoprotein, and RDRP, which is the other main responsible factor for the viral infection. The newly designed molecules showed better performance than several existing drugs. Conformational changes from the closed conformation to closed lock and open conformations of the spike protein and ACE 2 receptor upon interaction with the newly designed small molecules were observed. They also possess excellent drug scores and are non-toxic and non-mutagenic in comparison to the several existing antiviral molecules available in the market.

ASSOCIATED CONTENT

Supporting Information

The Supporting Information is available free of charge at https://pubs.acs.org/doi/10.1021/acs.jpcb.1c03294.

> Details of the methodology, related information for the complete understanding and reproducibility of the protocols, and source code links of all the bioinformatics tools used in this study (PDF)

AUTHOR INFORMATION

Corresponding Author

Chayan Kanti Nandi − *School of Basic Sciences, Indian Institute of Technology Mandi, Himachal Pradesh 175005, India;* orcid.org/0000-0002-4584-0738; Email: chayan@iitmandi.ac.in

Author

Pushpendra Mani Mishra − *School of Basic Sciences, Indian Institute of Technology Mandi, Himachal Pradesh 175005, India*

Complete contact information is available at:
https://pubs.acs.org/10.1021/acs.jpcb.1c03294

Notes

The authors declare no competing financial interest.

ACKNOWLEDGMENTS

REFERENCES

(1) Wang, C.; Wang, Z.; Wang, G.; Lau, J. Y.-N.; Zhang, K.; Li, W. COVID-19 in Early 2021: Current Status and Looking Forward. *Signal Transduct. Targets Ther.* **2021**, *6*, 114.

(2) Amanat, F.; Krammer, F. SARS-CoV-2 Vaccines: Status Report. *Immunity*; Cell Press, 2020, *52*, pp 583−589.

(3) The Lancet Respiratory Medicine. *Realising the Potential of SARS-CoV-2 Vaccines—a Long Shot? The Lancet Respiratory Medicine*; Lancet Publishing Group, 2021; p 117.

(4) COVID Research Updates: One Mutation Could Explain a Coronavirus Variant's Rampage. Nat. 2021, https://www.nature.com/articles/d41586-020-00502-w (accessed July 07, 2021).

(5) Zhou, Y.; Hou, Y.; Shen, J.; Huang, Y.; Martin, W.; Cheng, F. Network-Based Drug Repurposing for Novel Coronavirus 2019-NCoV/SARS-CoV-2. *Cell Discov.* **2020**, *6*, 14.

(6) White, K. M.; Rosales, R.; Yildiz, S.; Kehrer, T.; Miorin, L.; Moreno, E.; Jangra, S.; Uccellini, M. B.; Rathnasinghe, R.; Coughlan, L.; Martinez-Romero, C.; Batra, J.; Rojc, A.; Bouhaddou, M.; Fabius, J. M.; Obernier, K.; Dejosez, M.; Guillén, M. J.; Losada, A.; Avilés, P.; Schotsaert, M.; Zwaka, T.; Vignuzzi, M.; Shokat, K. M.; Krogan, N. J.; García-Sastre, A. Plitidepsin Has Potent Preclinical Efficacy against SARS-CoV-2 by Targeting the Host Protein EEF1A. *Science* **2021**, *371*, 926−931.

(7) Panda, P. K.; Arul, M. N.; Patel, P.; Verma, S. K.; Luo, W.; Rubahn, H.-G.; Mishra, Y. K.; Suar, M.; Ahuja, R. Structure-Based Drug Designing and Immunoinformatics Approach for SARS-CoV-2. *Sci. Adv.* **2020**, *6*, No. eabb8097.

(8) Mani Mishra, P.; Uversky, V. N.; Nandi, C. K. Serum Albumin-Mediated Strategy for the Effective Targeting of SARS-CoV-2. *Med. Hypotheses* **2020**, *140*, 109790.

(9) Wang, Y.; Zhang, D.; Du, G.; Du, R.; Zhao, J.; Jin, Y.; Fu, S.; Gao, L.; Cheng, Z.; Lu, Q.; Hu, Y.; Luo, G.; Wang, K.; Lu, Y.; Li, H.; Wang, S.; Ruan, S.; Yang, C.; Mei, C.; Wang, Y.; Ding, D.; Wu, F.; Tang, X.; Ye, X.; Ye, Y.; Liu, B.; Yang, J.; Yin, W.; Wang, A.; Fan, G.; Zhou, F.; Liu, Z.; Gu, X.; Xu, J.; Shang, L.; Zhang, Y.; Cao, L.; Guo, T.; Wan, Y.; Qin, H.; Jiang, Y.; Jaki, T.; Hayden, F. G.; Horby, P. W.; Cao, B.; Wang, C. Remdesivir in Adults with Severe COVID-19: A Randomised, Double-Blind, Placebo-Controlled, Multicentre Trial. *Lancet* **2020**, *395*, 1569−1578.

(10) Yu, W. L.; Toh, H. S.; Liao, C. T.; Chang, W. T. A Double-Edged Sword—Cardiovascular Concerns of Potential Anti-COVID-19 Drugs. *Cardiovascular Drugs and Therapy*; Springer June 17, 2020.

(11) Rebeaud, M. E.; Zores, F. SARS-CoV-2 and the Use of Chloroquine as an Antiviral Treatment. *Front. Med.* **2020**, *7*, 184.

(12) Jomah, S.; Asdaq, S. M. B.; Al-Yamani, M. J. Clinical Efficacy of Antivirals against Novel Coronavirus (COVID-19): A Review. *Journal of Infection and Public Health*; Elsevier Ltd., 2020, *13*, pp 1187−1195.

(13) Yoshimoto, F. K. The Proteins of Severe Acute Respiratory Syndrome Coronavirus-2 (SARS CoV-2 or n-COV19), the Cause of COVID-19. *Protein Journal*; Springer, 2020, *39*, pp 198−216.

(14) Dhama, K.; Khan, S.; Tiwari, R.; Sircar, S.; Bhat, S.; Malik, Y. S.; Singh, K. P.; Chaicumpa, W.; Bonilla-Aldana, D. K.; Rodriguez-Morales, A. J. Coronavirus Disease 2019−COVID-19. *Clin. Microbiol. Rev.* **2020**, *33*, 1−48.

(15) Li, F. Structure, Function, and Evolution of Coronavirus Spike Proteins. *Annu. Rev. Virol.* **2016**, *3*, 237−261.

(16) Yang, J.; Petitjean, S. J. L.; Koehler, M.; Zhang, Q.; Dumitru, A. C.; Chen, W.; Derclaye, S.; Vincent, S. P.; Soumillion, P.; Alsteens, D. Molecular Interaction and Inhibition of SARS-CoV-2 Binding to the ACE2 Receptor. *Nat. Commun.* **2020**, *11*, 1−10.

(17) Gil, C.; Ginex, T.; Maestro, I.; Nozal, V.; Barrado-Gil, L.; Cuesta-Geijo, M. Á.; Urquiza, J.; Ramírez, D.; Alonso, C.; Campillo, N. E.; Martinez, A. COVID-19: Drug Targets and Potential Treatments. *Journal of Medicinal Chemistry*; American Chemical Society, 2020, *63*, pp 12359−12386.

(18) Kevadiya, B. D.; Machhi, J.; Herskovitz, J.; Oleynikov, M. D.; Blomberg, W. R.; Bajwa, N.; Soni, D.; Das, S.; Hasan, M.; Patel, M.; Senan, A. M.; Gorantla, S.; McMillan, J.; Edagwa, B.; Eisenberg, R.; Gurumurthy, C. B.; Reid, S. P. M.; Punyadeera, C.; Chang, L.; Gendelman, H. E. Diagnostics for SARS-CoV-2 Infections. *Nat. Mater.* **2021**, *20*, 593−605.

(19) Lan, J.; Ge, J.; Yu, J.; Shan, S.; Zhou, H.; Fan, S.; Zhang, Q.; Shi, X.; Wang, Q.; Zhang, L.; Wang, X. Structure of the SARS-CoV-2 Spike Receptor-Binding Domain Bound to the ACE2 Receptor. *Nature* **2020**, *581*, 215−220.

(20) Sakkiah, S.; Guo, W.; Pan, B.; Ji, Z.; Yavas, G.; Azevedo, M.; Hawes, J.; Patterson, T. A.; Hong, H. Elucidating Interactions Between SARS-CoV-2 Trimeric Spike Protein and ACE2 Using Homology Modeling and Molecular Dynamics Simulations. *Front. Chem.* **2021**, *8*, 622632.

(21) Shoemark, D. K.; Colenso, C. K.; Toelzer, C.; Gupta, K.; Sessions, R. B.; Davidson, A. D.; Berger, I.; Schaffitzel, C.; Spencer, J.; Mulholland, A. J. Molecular Simulations Suggest Vitamins, Retinoids and Steroids as Ligands of the Free Fatty Acid Pocket of the SARS-CoV-2 Spike Protein. *Angew. Chem., Int. Ed.* **2021**, *60*, 7098−7110.

(22) Jiménez, J.; Doerr, S.; Martínez-Rosell, G.; Rose, A. S.; De Fabritiis, G. DeepSite: Protein-Binding Site Predictor Using 3D-Convolutional Neural Networks. *Bioinformatics* **2017**, *33*, 3036−3042.

(23) Goodfellow, I.; Pouget-Abadie, J.; Mirza, M.; Xu, B.; Warde-Farley, D.; Ozair, S.; Courville, A.; Bengio, Y.. Generative Adversarial Nets. *In Proceedings of the 27th International Conference on Neural Information Processing Systems*, 2014; Vol. 2, pp 2672−2680. https://papers.nips.cc/paper/2014/file/5ca3e9b122f61f8f06494c97b1afccf3-Paper.pdf (accessed July 07, 2021).

(24) Skalic, M.; Martínez-Rosell, G.; Jiménez, J.; De Fabritiis, G. PlayMolecule BindScope: Large Scale CNN-Based Virtual Screening on the Web. *Bioinformatics* **2019**, *35*, 1237−1238.

(25) Liu, Y.; Grimm, M.; Dai, W.-t.; Hou, M.-c.; Xiao, Z.-X.; Cao, Y. C B-Dock: A Web Server for Cavity Detection-Guided Protein−Ligand Blind Docking. *Acta Pharmacol. Sin.* **2020**, *41*, 138−144.

(26) Daina, A.; Michielin, O.; Zoete, V. SwissADME: A Free Web Tool to Evaluate Pharmacokinetics, Drug-Likeness and Medicinal Chemistry Friendliness of Small Molecules. *Sci. Rep.* **2017**, *7*, 1−13.

(27) Yang, J.-F.; Wang, F.; Chen, Y.-Z.; Hao, G.-F.; Yang, G.-F. LARMD: Integration of Bioinformatic Resources to Profile Ligand-Driven Protein Dynamics with a Case on the Activation of Estrogen Receptor. *Briefings Bioinf.* **2020**, *21*, 2206−2218.

(28) Schneidman-Duhovny, D.; Inbar, Y.; Nussinov, R.; Wolfson, H. J. PatchDock and SymmDock: Servers for Rigid and Symmetric Docking. *Nucleic Acids Res.* **2005**, *33*. DOI: DOI: 10.1093/nar/gki481.

(29) Andrusier, N.; Nussinov, R.; Wolfson, H. J. FireDock: Fast Interaction Refinement in Molecular Docking. *Proteins Struct. Funct. Genet* **2007**, *69*, 139−159.

(30) Sander, T.; Freyss, J.; Von Korff, M.; Reich, J. R.; Rufener, C. OSIRIS, an Entirely in-House Developed Drug Discovery Informatics System. *J. Chem. Inf. Model.* **2009**, *49*, 232−246.

(31) Zhu, J.-Y.; Zhang, R.; Pathak, D.; Darrell, T.; Efros, A. A.; Wang, E. S. O.. Toward Multimodal Image-to-Image Translation. *NIPS'17: Proceedings of the 31st International Conference on Neural Information Processing System*; 2017, pp 465−476.

(32) Skalic, M.; Jiménez, J.; Sabbadin, D.; De Fabritiis, G. Shape-Based Generative Modeling for de Novo Drug Design. *J. Chem. Inf. Model.* **2019**, *59*, 1205−1214.

(33) Trott, O.; Olson, A. J. AutoDock Vina: Improving the Speed and Accuracy of Docking with a New Scoring Function, Efficient Optimization, and Multithreading. *J. Comput. Chem.* **2009**, *31*, 455.

(34) Mashiach, E.; Schneidman-Duhovny, D.; Andrusier, N.; Nussinov, R.; Wolfson, H. J. FireDock: A Web Server for Fast Interaction Refinement in Molecular Docking. *Nucleic Acids Res.* **2008**, *36*, W229−W232.

(35) Guo, F.; Li, S.; Wang, L.; Zhu, D. Protein-Protein Binding Site Identification by Enumerating the Configurations. *BMC Bioinf.* **2012**, *13*, 158.